

Research papers

A demand-driven dynamic heating strategy for ultrafast and energy-efficient MgH₂ dehydrogenation utilizing the “burst effect”

Jianghao Cai^{a,b}, Yutong Jiang^{a,b}, Tongao Yao^{a,b}, Xiaotian Tang^{a,b}, Yuxuan Liu^{a,b},
Zhuoran Xu^{a,b}, Xiaojun Zhao^c, Bingdong Zhang^{a,b}, Zhengyang Gao^{a,b}, Weijie Yang^{a,b,*}

^a Hebei Key Laboratory of Energy Storage Technology and Integrated Energy Utilization, North China Electric Power University, Baoding 071003, Hebei, China

^b Department of Power Engineering, School of Energy, Power and Mechanical Engineering, North China Electric Power University, Baoding 071003, Hebei, China

^c Department of Electrical Engineering, School of Electrical and Electronic Engineering, North China Electric Power University, Baoding 071003, Hebei, China

ARTICLE INFO

Keywords:

Burst effect

MgH₂ dehydrogenation

Solid-state hydrogen storage

Numerical simulation

Thermal management

ABSTRACT

Magnesium hydride (MgH₂) holds immense potential for large-scale hydrogen storage due to its high gravimetric capacity and volumetric density. However, its practical application in energy storage systems is hindered by sluggish dehydrogenation kinetics and high energy consumption. Inspired by the burst effect in MgH₂ dehydrogenation, we proposed a demand-driven dynamic heating (DDDH) strategy that synchronizes thermal supply with reaction-stage-specific energy demands, aiming to simultaneously reduce dehydrogenation energy consumption and increase dehydrogenation rate. Based on experimental dehydrogenation curves, the variation curves of reaction rate parameters (activation energy and pre-exponential factor) with the dehydrogenation progress were obtained. The dehydrogenation processes of two typical devices (with and without fins) through traditional isothermal heating strategy and our newly proposed DDDH strategy were simulated. Numerical simulations of two reactor designs demonstrate that the DDDH strategy reduces dehydrogenation time by up to 57.99 % and improves exergy efficiency by 3.23 % at a peak temperature of 873 K and an equilibrium temperature of 573 K. These results demonstrate that the DDDH strategy is not only effective at the material level, but also suitable for system-level hydrogen release optimization under practical operating conditions. The DDDH strategy further demonstrates robust dehydrogenation performance under non-adiabatic conditions. Crucially, the strategy achieves these advancements without requiring additional hardware, enabling scalable deployment in stationery and grid-scale hydrogen energy storage systems. This work bridges material science and thermal engineering, offering a targeted solution to enhance the real-world applicability of solid-state hydrogen storage technologies in large-scale energy storage infrastructure.

1. Introduction

Hydrogen energy stands as a cornerstone for achieving global carbon neutrality due to its high energy density and zero-emission potential [1]. Large-scale hydrogen storage remains a critical challenge for integrating intermittent renewable energy sources into stable grid systems [2]. Solid-state hydrogen storage using magnesium hydride offers a compelling solution with high gravimetric (~7.6 wt%) and volumetric (~110 g/L) hydrogen storage densities and inherent safety under ambient conditions [3–5]. Despite these advantages the practical deployment of MgH₂-based systems is hindered by slow dehydrogenation kinetics and excessive energy demands [6,7]. Therefore, it is

essential to investigate the kinetic mechanisms of hydrogenation and dehydrogenation in magnesium-based hydrogen storage materials and to enhance these processes [8–11]. The challenges associated with magnesium-based hydrogen storage materials are determined by both heat transfer properties of the device and dehydrogenation kinetics of the material. Efforts are currently focused on optimizing the heat transfer performance of hydrogen storage tanks and reducing the activation energy of materials, respectively [12–14]. The performance of hydrogen storage tanks is primarily evaluated based on two criteria: energy consumption and rate.

To optimize the heat transfer performance of hydrogen storage tanks, researchers primarily focus on improving the tank structure, modifying relevant performance parameters, or employing advanced phase change

* Corresponding author at: Hebei Key Laboratory of Energy Storage Technology and Integrated Energy Utilization, North China Electric Power University, Baoding 071003, Hebei, China.

E-mail address: yangwj@ncepu.edu.cn (W. Yang).

<https://doi.org/10.1016/j.est.2025.117495>

Received 20 April 2025; Received in revised form 30 May 2025; Accepted 16 June 2025

Available online 19 June 2025

2352-152X/© 2025 Elsevier Ltd. All rights reserved, including those for text and data mining, AI training, and similar technologies.

Nomenclature*Symbols*

ε	porosity of MH bed
μ	dynamic viscosity, Pa s
λ	thermal conductivity, W/m/K
ψ	exergy efficiency
ξ	reaction process
ρ	density, kg/m ³
Ω	space computing region
ΔH	enthalpy change, kJ/mol H ₂
ΔS	entropy change, J/mol/K
A	pre-exponential factor
C_p	specific heat, J/kg/K
K	permeability, m ²
M	molar mass, g/mol
n	Avrami exponent

P	pressure, Pa
Q	heat flux, W/m ²
S	area, m ²
t	time, s
T	temperature, K
u	velocity, m/s
wt	maximum hydrogen density, wt%

Subscripts

d	dehydrogenation
eq	equilibrium
eff	effective
gas	gas
out	outlet
s	solid
ref	reference
w	wall

materials. Numerical modeling of hydrogen storage tanks with MgH₂ composite compression disks demonstrated that increasing hydrogen supply pressure to 2.6 MPa and heat transfer fluid (HTF) velocity to 5 m/s significantly accelerated dehydrogenation kinetics [15]. Subsequently, comparative analysis of metal hydride thermal energy storage systems demonstrated that compacting MH powder enhances bed thermal conductivity, as validated by gravimetric heat storage rate (GHSR) maximization [16]. Comparative studies installing helical coil heat exchangers (HCHes) in tank systems demonstrated their superiority over conventional designs through enhanced thermal performance and validated operational efficiency [17,18]. In addition to modifying the heat exchanger structure, changing the material is another viable option. A novel sandwich-structured MH-TCM hydrogen storage system achieved a 61.1 % reduction in hydrogen storage duration by optimizing thermochemical material distribution to 40 % inner-layer volume ratio, expanding heat transfer area while minimizing thermal resistance [19]. Optimized thermal management via high-temperature hydrogen gas as both heat transfer medium and reactant in a Mg-based storage system enabled efficient hydrogen absorption at 473 K and desorption at 773 K, with a 9:1 structural height ratio and increased flow rates accelerating kinetics, while coupling to a gas circulatory system established an integrated framework for scalable solid-state hydrogen storage [20].

To optimize the intrinsic properties of materials, researchers primarily employ strategies such as adding catalysts, nano-structuring, or alloying. It has been demonstrated that doping with K₂TaF₇ improves the hydrogen storage performance of MgH₂ by lowering the dehydrogenation temperature, reducing activation energy, and enhancing reversible capacity through synergistic catalytic effects [21]. Similarly, the use of high-entropy alloys has been reported to significantly enhance the hydrogen storage properties of MgH₂, exhibiting exceptional catalytic activity, accelerating dehydrogenation kinetics, and reducing operational temperatures [22]. Studies have shown that the Ni₆MnO₈@rGO nanocomposite enhances MgH₂ hydrogen sorption by lowering temperatures, reducing activation energies, and improving cyclic stability through synergistic catalytic effects [23]. In addition, FeCoNiCrTi high-entropy alloy (HEA) nanosheets have been found to improve MgH₂ hydrogen storage, reducing the dehydrogenation temperature to 471.5 K and decreasing the activation energy by 51 % through synergistic catalysis [24]. Two-dimensional V₂C MXene significantly enhances MgH₂ hydrogen storage performance by lowering the onset desorption temperature to 463 K, reducing activation energy, and slightly decreasing reaction enthalpy [25]. Yttrium addition to Mg alloys also improves hydrogen absorption kinetics and desorption rates. Mg₂₄Y₃ shows optimal performance and the lowest dehydrogenation activation energy, although it leads to a slight reduction in reversible

hydrogen capacity [26].

Despite extensive research focusing separately on improving heat transfer or modifying material properties, integrated performance optimization remains insufficient for meeting the requirements of large-scale hydrogen storage systems. This is primarily because research has typically been conducted in isolation, whereas this is an interdisciplinary field that requires a simultaneous and synergistic approach to optimize both material properties and heat transfer characteristics. In heat and mass transfer studies, greater attention should be paid to the variations in material properties. Research has shown that dehydrogenation kinetics are dynamic, which presents new possibilities and challenges for the study of heat transfer characteristics. Kapischke et al., [27] for the first time, used a measuring technique with oscillating change of temperature in a non-permeated packed bed of fine-grained material and found that the thermal-physical property of the MgH₂ bed changed with temperature. The growth behavior of magnesium during the dehydrogenation of MgH₂ nanoparticles has been studied, revealing a unique transition mechanism [28]. The growth of Mg microcrystals occurs in three stages, with a slower dehydrogenation rate in the first stage and an accelerated rate in the second stage. In our previous study [29], layer-by-layer calculations of the MgH₂ dehydrogenation process were performed using density functional theory and molecular dynamics. We found that the energy barrier for dehydrogenation from the surface layer of MgH₂ is initially the highest, then decreases and stabilizes. This reduction in the energy barrier, along with an increase in the reaction rate, indicates a transition from slower to faster dehydrogenation. Based on the burst effect, the first kinetic prediction model for solid-state hydrogen storage was proposed [30]. These findings emphasize that understanding the interaction between material-level kinetics and system-level thermal response is crucial for achieving high-performance solid-state hydrogen storage systems suitable for grid-scale deployment.

In summary, the external device design and internal material modification form an integrated system. However, at present, they are being optimized separately to reduce energy consumption or improve the rate. These aspects should be synergized to more effectively address the challenge. To address this gap, and to support the development of scalable hydrogen storage technologies, we draw on the burst effect of MgH₂ dehydrogenation and propose the demand-driven dynamic heating (DDDH) strategy that synchronizes thermal supply with reaction-stage-specific energy demands, aiming to simultaneously reduce dehydrogenation energy consumption and increase dehydrogenation rate. Firstly, the segmented kinetic characteristic curves of MgH₂ dehydrogenation were obtained. Subsequently, two typical devices (with and without fins) were selected to simulate the dehydrogenation process

using both the conventional isothermal heating strategy and our newly proposed demand-driven dynamic heating strategy. The energy demand variations during the dehydrogenation reaction were subsequently analyzed. The dehydrogenation energy consumption and rate were compared under both heating strategies. Additionally, for the demand-driven dynamic heating strategy, the effects of the peak temperature and final temperature of dehydrogenation on energy consumption and rate were examined. Although the DDDH strategy involves a higher peak dehydrogenation temperature, it achieves better overall energy utilization and significantly enhances the practical efficiency of MgH_2 storage systems. This novel heating strategy can significantly improve the energy utilization and dehydrogenation rate of the device by adjusting the temperature, without requiring additional equipment. As such, the DDDH approach provides a practical and scalable solution for advancing magnesium-based solid-state hydrogen storage technologies toward real-world applications in large-scale energy storage.

2. Mathematical model

The two-dimensional metal hydride reactors considered in this study are illustrated in Fig. 1. Both the reactor body and the circular fins are constructed from brass and filled with magnesium hydride powder. The two reactor models differ in their internal fin configurations, designed to explore the influence of heat transfer structures. In the thermal boundary setup, heat flux is applied to the lateral wall, the bottom surface, and the top surface, except for the localized area of the hydrogen outlet, which is modeled as thermally insulated. This heating layout reflects realistic configurations where external heaters or contact surfaces are used to promote uniform heating. Detailed geometric and material parameters are presented in Fig. S1. Hydrogen acts as both the heat and mass transfer medium, entering the tank through the inlet during absorption, and is desorbed and released through the outlet during the dehydrogenation process.

The hydrogen dehydrogenation processes in MH reactors are described using energy and mass balance equations, along with thermodynamic and kinetic models. The general assumptions include: (1) Hydrogen is treated as an ideal gas; (2) The physical properties of the material are constant throughout the reaction, unless otherwise specified; (3) Local equilibrium is assumed between the MH and hydrogen gas; (4) The MH beds are treated as porous media with uniformly

distributed particles and constant porosity; (5) The volume expansion of particles and internal stresses within the MH beds are neglected; (6) The reactor is well insulated, preventing heat transfer with its surroundings.

2.1. Heat transfer equations

The heat transfer equation for the porous hydrogen storage material reactor bed is follows [31]:

$$(\rho C_p)_{eff} \frac{\partial T_s}{\partial t} + \rho_g C_{p,g} u_g \nabla T_s = \nabla (\lambda_{eff} \nabla T_s) + S_T \quad (1)$$

where ρ_g is the density of hydrogen gas, $C_{p,g}$ is the specific heat capacity of hydrogen gas, u_g stands for the velocity of hydrogen gas. λ_{eff} represents effective thermal conductivity, $(\rho C_p)_{eff}$ stands for effective volumetric heat capacity, and S_T denotes internal heat source, as defined below [32]:

$$\lambda_{eff} = \varepsilon \lambda_g + (1 - \varepsilon) \lambda_s \quad (2)$$

$$(\rho C_p)_{eff} = \varepsilon \rho_g C_{p,g} + (1 - \varepsilon) \rho_s C_{p,s} \quad (3)$$

$$S_T = \rho_{emp} wt (1 - \varepsilon) \left[\frac{\Delta H}{M_g} + T_s (C_{p,g} - C_{p,s}) \right] \frac{d\xi}{dt} \quad (4)$$

where λ_s , ρ_s and $C_{p,s}$ are the thermal conductivity, density, specific heat capacity of the MH bed, ε represents the porosity of the MH bed, M_g presents the molar mass of hydrogen, and wt stands for the maximal hydrogen concentration in the Mg-based MH.

Energy equation for the heat exchanger tube wall:

$$\rho_w C_{p,w} \frac{\partial T_w}{\partial t} = \nabla (\lambda_w \nabla T_w) \quad (5)$$

where λ_w , ρ_w and $C_{p,w}$ are the thermal conductivity, density, specific heat capacity of the copper wall and fins.

2.2. Mass transfer equations

The mass transfer equation between hydrogen and Mg-based MH can be expressed as [33]:

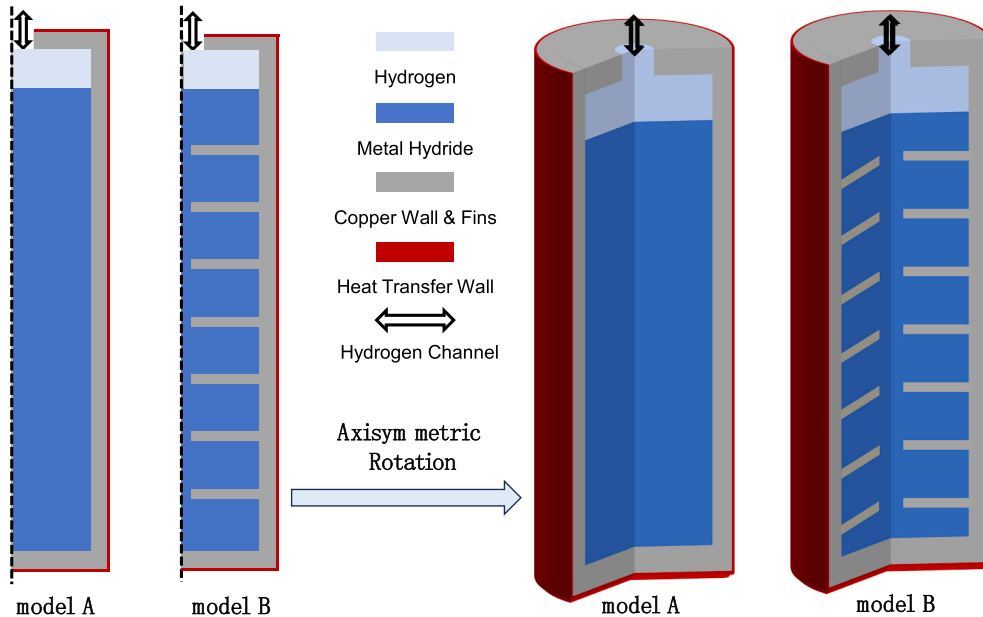


Fig. 1. Schematic structure of hydrogen storage tank model.

$$\frac{\partial \varepsilon \rho_g}{\partial t} + \nabla(\rho_g u_g) = S_m \quad (6)$$

where S_m is the mass source of dehydrogenation reaction, as defined below [34]:

$$S_m = \rho_{emp} w t (1 - \varepsilon) \frac{d\xi}{dt} \quad (7)$$

The Mg-based MH is treated as porous medium, and the Darcy's law is used to describe the hydrogen flow within the hydrogen bed:

$$u_g = -\frac{K}{\mu_g} \nabla P_g \quad (8)$$

Here, u_g is the flow velocity of hydrogen, K is the permeability, P_g is the pressure, and μ_g is the dynamic viscosity of hydrogen, which can be expressed as $\mu_g = 9.05 \times 10^{-5} \left(\frac{T}{293}\right)^{0.68}$.

2.3. Dehydrogenation reaction kinetic equations

The reaction process of dehydrogenation in a hydrogen storage tank can be expressed as ξ versus time, with the reaction fraction ξ going from 0 to 1. The reaction process can be represented by the Johnson-Mehl-Avrami-Kolmogorov (JMAK) model [35]. The JMAK model shows a very high level of fit in modeling the dehydrogenation process of magnesium-based hydrogen storage materials, which is shown below:

$$\xi = 1 - e^{-(kt)^n} \quad (9)$$

$$\ln(-\ln(1 - \xi)) = n \ln k + n \ln t \quad (10)$$

Here, n is the Avrami exponent, k is the reaction rate parameter which is related to T , P_g , A_d and E_d , which is shown as [36–39]:

$$k = A_d \exp\left(-\frac{E_d}{R_g T_s}\right) \ln\left(\frac{P_g}{P_{eq,d}}\right), P_{eq,d} > P_g \quad (11)$$

The hydrogenation reaction occurs when the hydrogen equilibrium

pressure is lower than the reaction pressure. Conversely, when the hydrogen equilibrium pressure exceeds the reaction pressure, the dehydrogenation reaction takes place. The relationship between the hydrogen equilibrium pressure and the reaction temperature is shown below [40–43]:

$$\ln\left(\frac{P_{eq}}{P_{ref}}\right) = \frac{\Delta H}{R_g T_s} - \frac{\Delta S}{R_g} \quad (12)$$

where P_{ref} denotes the reference pressure, usually considered to be 0.1 MPa. Therefore, the dehydrogenation kinetic equation can be expressed as [44–46]:

$$\frac{d\xi}{dt} = A_d \exp\left(-\frac{E_d}{R_g T_s}\right) \ln\left(\frac{P_g}{P_{eq,d}}\right) n (1 - \xi) [-\ln(1 - \xi)]^{\frac{n-1}{n}} \quad (13)$$

Inspired by the burst effect observed in MgH₂ dehydrogenation, we first conducted a segmented analysis of the dehydrogenation kinetics using the JMAK model. In this process, the reaction progression was divided into 5% intervals, and the pre-exponential factor and activation energy were independently calculated for each segment based on experimental data. This segmentation revealed clear changes in kinetic behavior, particularly a steep decrease in activation energy at the beginning of the reaction which supports the “burst effect” mechanism proposed in our earlier work [29,30]. The segmented results, although initially discontinuous, showed high agreement with experimental dehydrogenation curves, as seen in Figs. 2(a) and S3(c).

To construct a more realistic and continuous kinetic model suitable for numerical simulation, the segmented kinetic parameters were fitted using an exponential decay function (ExpDec3). This smoothing procedure resulted in continuous functions for both activation energy and the pre-exponential factor, shown in Fig. 2(b) and (c). The fitted functions are given in Eqs. (14) and (15), with high correlation coefficients ($R^2 = 0.970$ and 0.965), indicating strong consistency with the segmented data and underlying physical behavior.

$$\ln(A_d) = 17.13 \times \exp\left(-\frac{\xi}{0.075}\right) + 10.90 \quad (14)$$

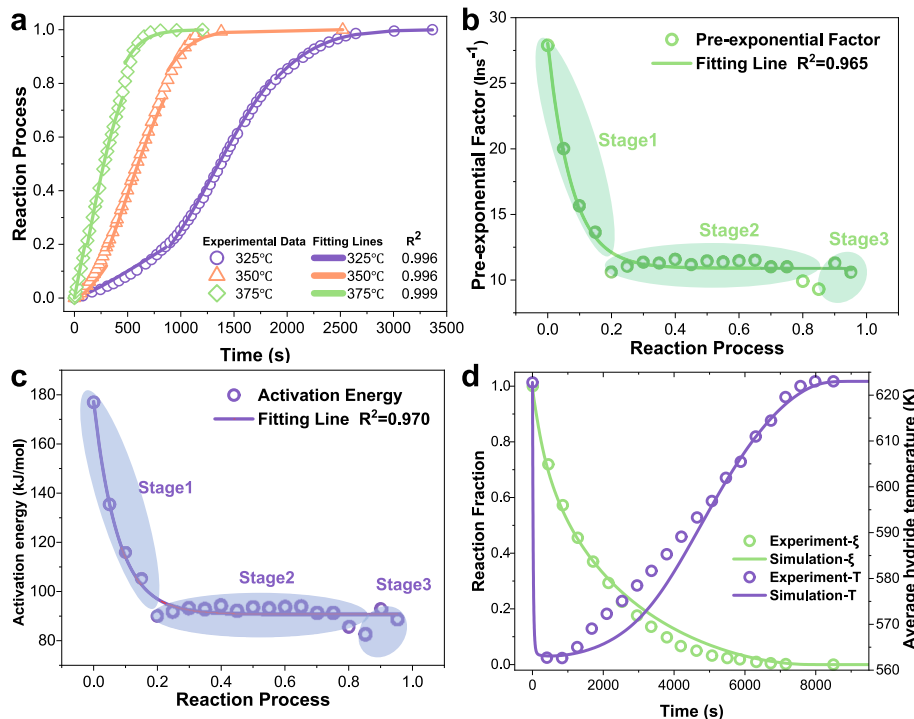


Fig. 2. (a) Dehydrogenation fitting curves using segmented results. Fitted function curves of (b) dehydrogenation pre-exponential factor and (c) activation energy during dehydrogenation of magnesium hydride and (d) Comparison of simulation results with experimental results [31] at 623 K dehydrogenation temperature.

$$E_d = 86.50 \times \exp\left(-\frac{\xi}{0.076}\right) + 90.68 \quad (15)$$

2.4. Energy consumption calculation equation

To facilitate the calculation of energy consumption during the dehydrogenation process, a second-type boundary condition is adopted in this study, in which a prescribed heat flux Q is applied to the tank walls. The constant heat flux boundary allows for direct control of thermal input and is also more responsive and easier to implement in electrically heated systems. In addition, the use of a second-type boundary condition simplifies the quantification of energy input, which is essential for subsequent energy and exergy analyses. Under the assumption of adiabatic surroundings, all heat flux from the walls is absorbed internally by the tank structure and the hydride bed. The heat absorbed by the bed can be divided into two parts: one associated with the heating phase, and the other with the endothermic chemical reaction. The total theoretical energy required by the hydrogen storage tank is defined by Eq. (16).

$$E = QSt = \sum_i \int_{\Omega_s} (\rho C_p)_e (T_i - T_{i-1})_s dV + \sum_i \int_{\Omega_w} (\rho C_p)_w (T_i - T_{i-1})_w dV + \sum_i \int_{\Omega_s} S_m \left[\frac{\Delta H}{M_g} + T_{i,s} (C_{p,g} - C_{p,s}) \right] dV \quad (16)$$

where S denotes the heated area, which for both models is the entire outer surface. Ω is denoted as a space region. The subscripts i , s , w , and g denote the time step, the hydride, the hydrogen storage tank, and the hydrogen, respectively.

2.5. Exergy analysis of dehydrogenation process

For practical applications, it is crucial to assess not only the energy content but also its efficiency [47]. Analysis of the exergy of dehydrogenation device is very important. The exergy input to the device is obtained by Eq. (17).

$$Ex_{in} = QSt \quad (17)$$

The exergy in the dehydrogenation reaction is calculated by Eq. (18):

$$Ex_{des} = \sum_i \left\{ \int_{\Omega_s} (\rho C_p)_e (T_i - T_{i-1})_s + S_m \left[\frac{\Delta H}{M_g} + T_{i,s} (C_{p,g} - C_{p,s}) \right] dV \right\} \left(1 - \frac{300}{T_{i,s}} \right) \quad (18)$$

The exergy efficiency can be obtained from Eq. (19) [48–51]:

$$\psi = \frac{Ex_{des}}{Ex_{in}} \quad (19)$$

2.6. Initial and boundary conditions

The initial temperature for dehydrogenation is 300 K, with a constant hydrogen supply pressure of 0.1 MPa. The hydrogen inlet and outlet satisfy the adiabatic boundary conditions as follows:

$$\frac{\partial T_g}{\partial \vec{n}} = 0 \quad (20)$$

The initial hydrogen pressure of hydrogen in the hydrogen storage tank is satisfied:

$$P_g = P_{eq,d} \quad (21)$$

Table 1

Physical parameters of the model in this work.

Parameters		Values
ΔH	Reaction enthalpy of Mg-based MH	75,000 J/mol H ₂
ΔS	Reaction entropy of Mg-based MH	135.6 J/mol/K
M_g	The molar mass of hydrogen	2.01588 kg/kmol
w_t	The maximal hydrogen concentration	0.06
ε	Porosity	0.74
ρ_{emp}	Density of the Mg-based MH	1800 kg/m ³
λ_g	Thermal conductivity of hydrogen	0.167 W/m/K
$C_{p,g}$	Specific heat of hydrogen	14,890 J/kg/K
λ_s	Thermal conductivity of hydride	0.48 W/m/K
$C_{p,s}$	Specific heat of hydride	1545 J/kg/K
K	Permeability	5.75×10^{-12} m ²
λ_w	Thermal conductivity of tank (Brass)	8430 W/m/K
$C_{p,w}$	Specific heat of tank (Brass)	385.2 J/kg/K
ρ_w	Density of tank (Brass)	108.9 Kg/m ³

Other symmetric or adiabatic boundaries can be expressed as:

$$\frac{\partial T_s}{\partial \vec{n}} = \frac{\partial T_w}{\partial \vec{n}} = \frac{\partial T_g}{\partial \vec{n}} = 0 \quad (22)$$

2.7. Numerical implementation

The physical parameters used in the simulation are summarized in Table 1. The model was solved using the commercial software package COMSOL Multiphysics 6.2. In this study, both Model A and Model B were analyzed using a two-dimensional, axisymmetric model. The relative and absolute errors were set to 10^{-4} . For the heat transfer component, the solid and fluid heat transfer module was used, while Darcy's law was applied for the mass transfer component. Additionally, the ordinary differential equations and algebraic differential equations modules were employed to model the dynamics. As shown in Fig. S2, a comparison of several mesh sizes demonstrated that a 1 mm mesh size provided both computational accuracy and efficiency. Therefore, a 1 mm mesh size was selected for the simulations.

By establishing a consistent set of simulation parameters, the temporal evolution of both average temperature and hydrogen mass fraction during dehydrogenation was numerically investigated. As shown in Fig. 2(d), the simulation results demonstrate reasonable consistency with experimental measurements [31], with the most significant deviation occurring between 2000 and 4000 s. This discrepancy may be

partially attributed to measurement inaccuracies in experimental average temperature coupled with inadequate consideration of intrinsic dynamic material properties in the simulation parameters. The enhanced correlation with experimental data achieved by the dynamic parameters suggests improved model fidelity. These findings collectively confirm the validity and reliability of the proposed mathematical framework, which incorporates both material-specific characteristics and simulation-based validation.

3. Results and discussion

3.1. The demand-driven dynamic heating (DDDH) strategy

The dehydrogenation process of MgH₂ exhibits a dynamic energy barrier, which decreases during the reaction and then stabilizes. This behavior, known as the burst effect, causes the temperature requirement

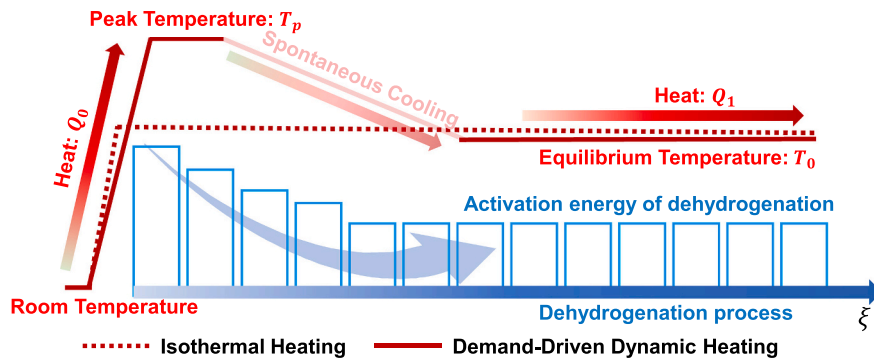


Fig. 3. Schematic of the demand-driven dynamic heating (DDDH) strategy.

to vary over time. However, previous studies [3,15–20,31–44,52,53] have typically applied a constant reaction temperature throughout the process, potentially resulting in excessive energy use or insufficient thermal input. To address this, we propose a demand-driven dynamic heating (DDDH) strategy based on the evolving reaction kinetics, as illustrated in Fig. 3. The approach begins by applying a constant heat flux Q_0 to the tank wall, which rapidly raises the system temperature to a defined peak temperature T_p . Once the hydride bed reaches the minimum reaction threshold, dehydrogenation initiates. The high wall temperature helps overcome the initial energy barrier, accelerating the reaction [54,55].

The system maintains T_p until the reaction reaches 20 % completion. At that point, heat input is stopped. Due to the adiabatic condition, internal heat is redirected entirely to support the chemical reaction. As the temperature naturally drops to a lower equilibrium value T_0 , a smaller heat flux Q_1 is applied to maintain that temperature until dehydrogenation completes. The full thermal management process is described by the strategy equation in Eq. (23). All boundary conditions used in this study remain within the safe operational limits of both the hydride material and tank structure.

$$Q = \begin{cases} Q_0, T_w < T_p, \xi < 0.2 \\ 0, T_0 < T_w < T_p, \xi \geq 0.2 \\ Q_1, T_w < T_0, \xi \geq 0.2 \end{cases} \quad (23)$$

3.2. Isothermal dehydrogenation performance under varying temperature conditions

The first scenario investigates isothermal dehydrogenation under controlled wall heat flux conditions. The procedure for selecting the optimal heat flux Q is detailed in Fig. S4 of the Supporting Information. Once thermal equilibrium is reached at the wall boundary, the system maintains steady operating conditions throughout the dehydrogenation process. While Model A and Model B exhibit similar overall behavior, Model B is more commonly used in engineering applications and is thus the main focus of this study. Additional specifications and performance data for Model A are provided in Fig. S5.

Fig. 4 illustrates the thermal performance of Model B under different wall temperature settings, comparing average bed temperature, reaction fraction, and energy consumption. As shown in Fig. 4(a), temperature evolution follows three distinct stages: a rapid initial rise, a brief cooling

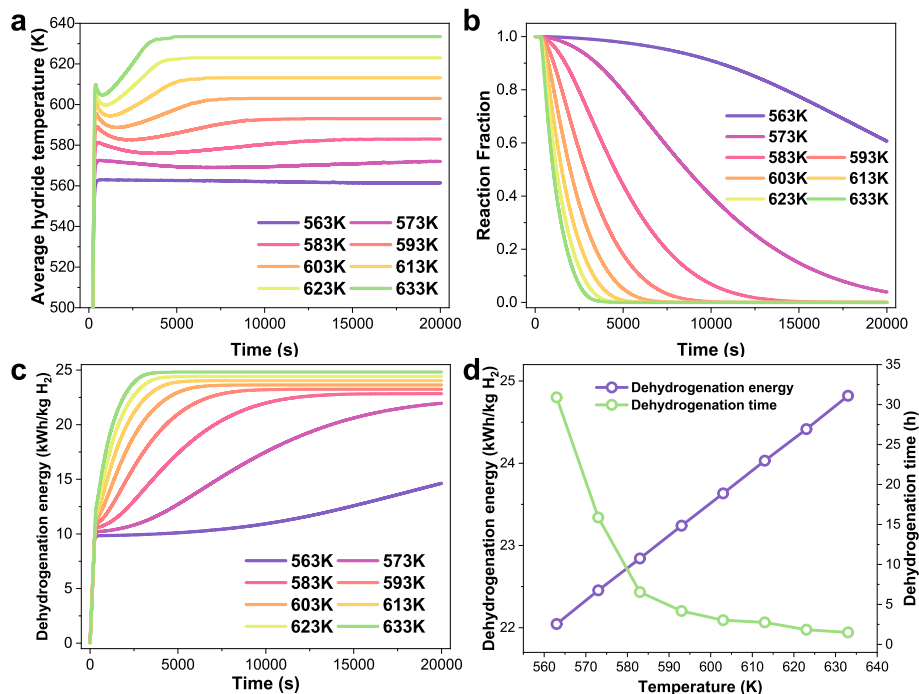


Fig. 4. At different dehydrogenation temperatures, the curves of (a) average hydride temperature, (b) reaction fraction and (c) dehydrogenation energy variation with reaction time, (d) energy consumption and time of dehydrogenation versus reaction temperatures for Model B at 10 kW/m^2 .

phase during early dehydrogenation, and gradual reheating until completion [56–58]. In Fig. 4(b), the reaction progress closely follows the temperature profile over time. Fig. 4(c) shows that increasing the wall temperature from 563 K to 633 K shortens the dehydrogenation time by 29.4 h and reduces energy consumption by 2.77 kWh/kg H₂. Fig. 4(d) presents the cumulative energy consumption, which increases sharply at first due to heating of the hydride, then stabilizes as the endothermic reaction becomes dominant. Compared to Model A (Fig. S5), Model B consumes more energy, mainly due to its larger tank mass, which requires additional heating. The differences in reaction energy across temperature settings are primarily attributed to heat absorbed by the tank structure. Finally, Fig. S6 presents transient contour plots of temperature and hydrogen concentration fields, confirming that the optimized geometry of Model B enhances thermal uniformity during the reaction.

3.3. Effect of different peak temperatures with the DDDH strategy

The second case considers variable-temperature dehydrogenation using the DDDH strategy, with heat flux settings detailed in Figs. S7–S9. Fig. 5(a) shows the evolution of average hydride temperature in Model B over time at different peak temperatures (T_p). As T_p increases, the hydride bed heats more rapidly before cooling to the equilibrium temperature, following a similar trend across all cases. As shown in Fig. 5(b), a higher T_p accelerates the dehydrogenation process and enhances hydrogen release during the subsequent cooling stage, highlighting a performance advantage over isothermal heating.

Compared to Model A, Model B achieves faster hydrogen release and shorter reaction time across all temperatures, due to its enhanced thermal conductivity [59,60]. However, this benefit comes with increased energy consumption, primarily due to the greater mass of the tank. The total energy consumption for Model B is 22.45 kWh/kg H₂,

distributed as 9.30 % for the hydride, 35.30 % for the tank, and 55.40 % for the chemical reaction. While the energy used by the hydride and chemical reaction slightly decreases due to lower hydride mass, the contribution of tank increases significantly due to its structural bulk.

The energy-time profile in Fig. 5(c) consists of three stages. Initially, energy increases rapidly as heat is absorbed by the tank and hydride. Once the threshold temperature is reached, the reaction initiates and energy are directed to the chemical process. In the second stage, a plateau appears around 20 % of dehydrogenation is completed with no external heating, as the tank releases stored heat to maintain the reaction. In the final stage, heat is reapplied to maintain equilibrium temperature, while the reaction rate gradually slows due to decreasing hydrogen content. Fig. 5(d) further illustrates this energy behavior in Model B. The graph shows an initial sharp rise, a plateau at 20 % dehydrogenation, and a gradual increase as the reaction progresses. No heat is applied during the plateau, as internal tank heat sustains the reaction.

3.4. Effect of different equilibrium temperatures with the DDDH strategy

Fig. 6 illustrates the performance of Model B at various equilibrium temperatures. As shown in Fig. 6(a), all parameters remain constant except for the equilibrium temperature, resulting in identical curves until the hydrogen storage tank reaches thermal equilibrium. A higher equilibrium temperature enables the target tank temperature to be reached more rapidly, thus initiating the temperature maintenance phase earlier. Fig. 6(b) demonstrates that the lower hydride temperatures associated with the conventional strategy led to slower dehydrogenation rates and extended dehydrogenation durations.

Fig. 6(c) shows that the DDDH strategy does not significantly affect total energy consumption, regardless of the equilibrium temperature. Under the isothermal heating strategy, the hydrogen storage tank

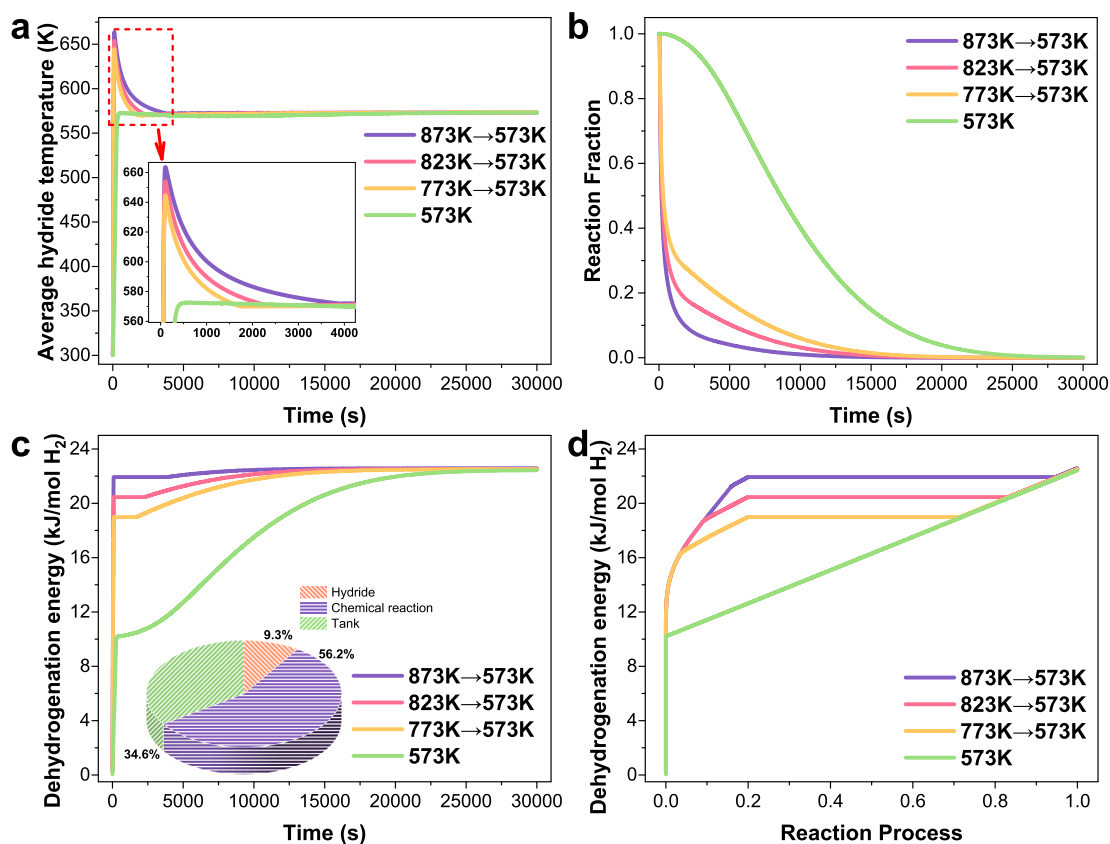


Fig. 5. Variation of (a) reaction time versus average hydride temperature, (b) reaction time versus reaction fraction, (c) reaction time versus dehydrogenation energy and (d) reaction process versus reaction energy at different peak temperatures for Model B.

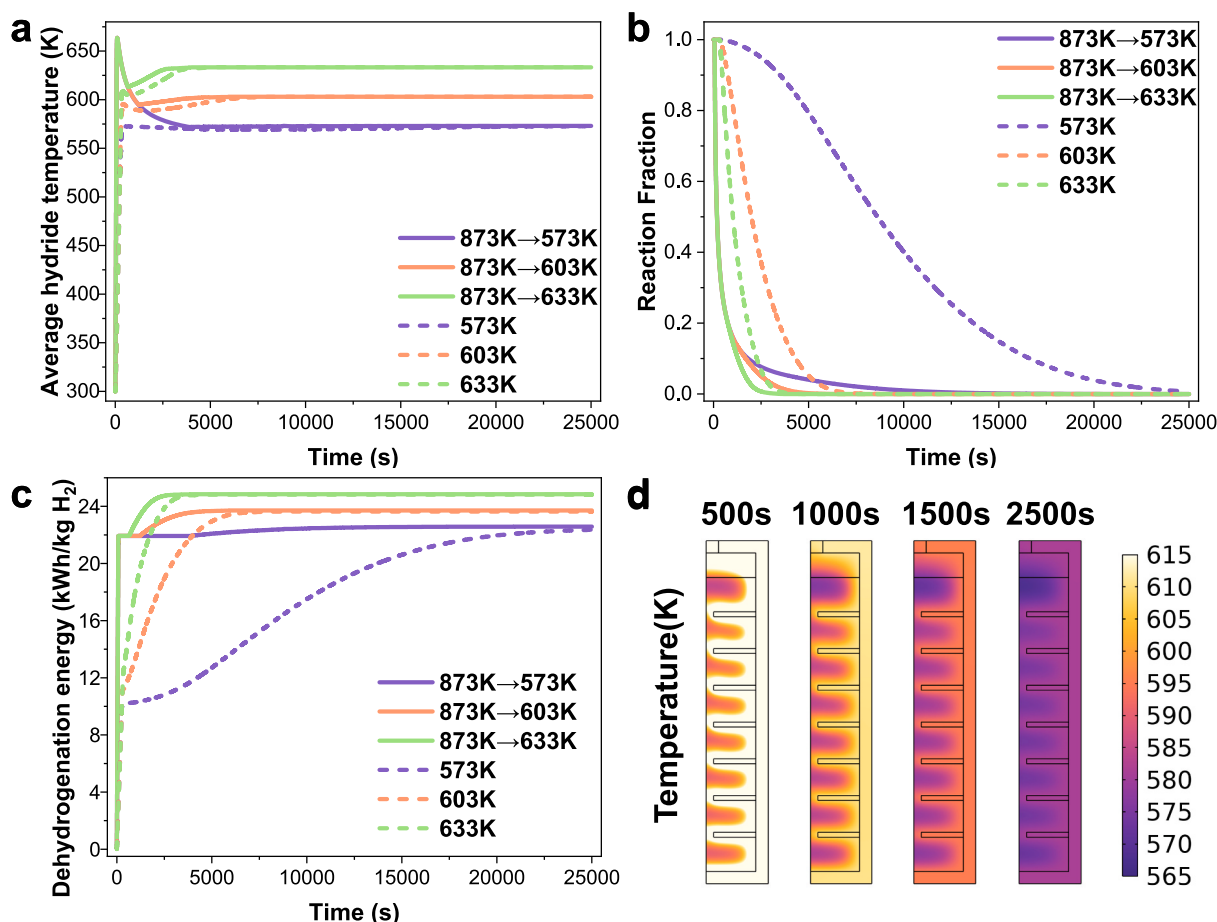


Fig. 6. Variation of (a) reaction time versus average hydride temperature, (b) reaction time versus reaction fraction and (c) reaction time versus reaction energy and (d) temperature contour plots during dehydrogenation for Model B.

reaches a lower temperature, reducing energy consumption during the initial dehydrogenation phase. However, energy expenditure increases in later stages due to the substantial heat absorption required for the dehydrogenation reaction, which supplies the energy necessary for chemical transformation. In contrast, the DDDH strategy causes the hydrogen storage tank to reach a considerably higher temperature earlier in the process, resulting in greater initial energy consumption for the device as a whole. The main advantage of this approach is the acceleration of the dehydrogenation process, as the higher initial temperature effectively overcomes the energy barrier inherent in magnesium-based hydrogen storage materials, thereby significantly accelerating the reaction [61]. Meanwhile, Fig. 6(d) represents the temperature contour plots inside the hydrogen storage tank for different reaction times. Similarly, the trends observed for Model A (Fig. S11) are consistent with those of Model B. This further supports the generalizability of the results and confirms that the DDDH strategy yields similar performance improvements across both models.

3.5. Comparative assessment of energy consumption and exergy efficiency in dehydrogenation processes

In this study, energy consumption is primarily determined by the final equilibrium temperature. The DDDH strategy effectively reduces energy demand while significantly shortening dehydrogenation time. As shown in Fig. 7(a), Model A achieves limited energy savings under DDDH due to its lower thermal conductivity. For example, energy consumption is reduced by 0.31 and 0.50 kWh/kg H₂, corresponding to savings of 0.67 % and 0.78 %, respectively. In contrast, Fig. 7(b) shows that Model B achieves more substantial reductions. When transitioning

from 873 K to 603 K, the dehydrogenation time decreases to approximately 1.10 h, and energy consumption is reduced to 0.67 kWh/kg H₂ (2.98 %). Similarly, transitioning to 573 K results in a time of 2.81 h and consumption of 0.78 kWh/kg H₂ (3.49 %). These values outperform those observed in constant-temperature scenarios at 588 K and 593 K. These results indicate that at higher equilibrium temperatures, the DDDH strategy primarily contributes to energy savings, while at lower temperatures, it mainly accelerates the dehydrogenation process.

For both models, the energy used to heat the hydride and to support the chemical reaction is defined as effective energy input [62,63]. Fig. 7 (c) and (d) illustrate the exergy efficiencies under various heating conditions. Without the DDDH strategy, exergy efficiencies remain relatively low: 0.31 for Model A and 0.29 for Model B. The slightly lower efficiency of Model B results from its higher energy requirement for structural heating. Adjusting dehydrogenation temperature alone has minimal influence on exergy performance. However, when the DDDH strategy is applied with a higher peak temperature (such as 873 K), the exergy efficiency improves significantly. Specifically, it increases by 1.26 % in Model A and by 3.23 % in Model B. These improvements are particularly relevant for large-scale hydrogen storage systems, where enhanced energy efficiency directly contributes to sustainability and cost-effectiveness.

3.6. Comparative assessment of reaction time in dehydrogenation processes

When the hydrogen storage tanks reach thermal equilibrium and are insulated from external heat exchange, all available heat is used to raise the material temperature and drive the endothermic reaction. As a

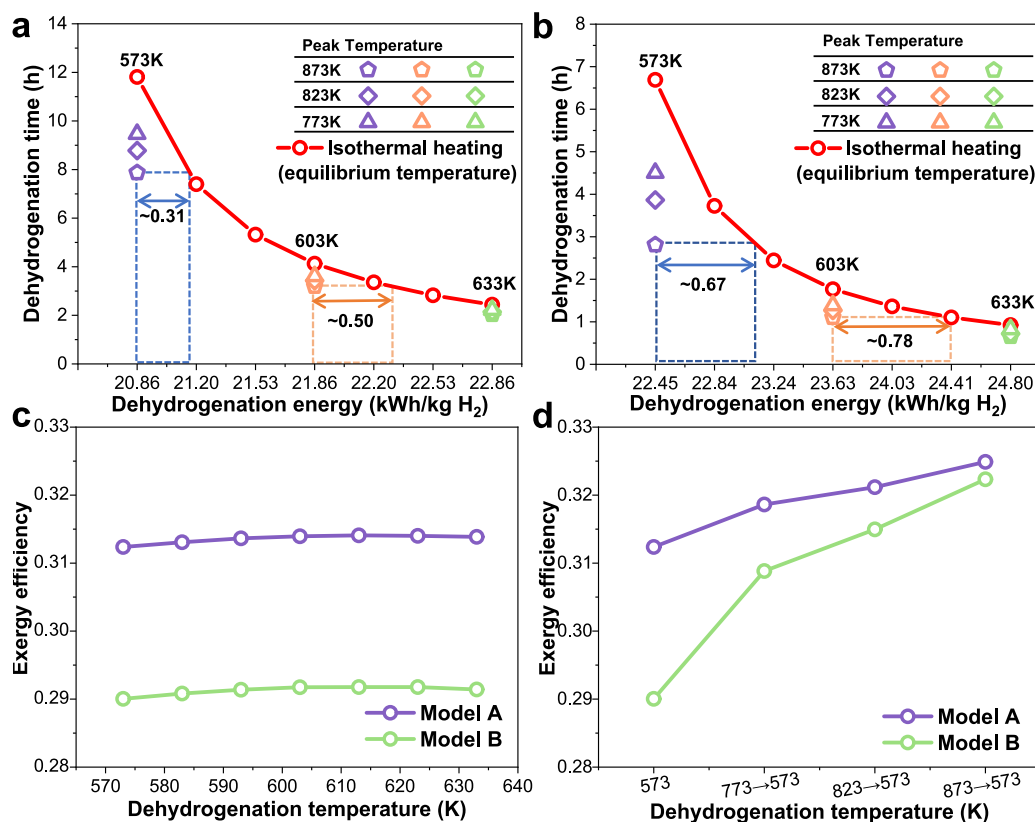


Fig. 7. Optimization of energy consumption of different dehydrogenation strategies for (a) Model A (without fins), (b) Model B (with fins). Exergy analysis of dehydrogenation process for (c) isothermal heating, (d) demand-driven dynamic heating.

result, for a given equilibrium temperature, the energy required for dehydrogenation remains constant. Fig. 8(a) and (b) present the optimization of dehydrogenation time for different strategies in Model A and Model B. At the same equilibrium temperature, energy use remains unchanged. Due to the “burst effect” in magnesium hydride, a higher initial temperature can more effectively overcome the activation barrier, thereby speeding up the reaction and shortening the overall duration. For Model A, the DDDH strategy reduces reaction time by 33.36 %, 22.33 %, and 16.39 % at 573 K, 603 K, and 633 K, respectively. Due to its better heat transfer, Model B shows even greater time savings: 57.99 %, 37.85 %, and 28.26 %. However, the time-saving benefit declines as the equilibrium temperature increases.

Fig. 8(c) summarizes how different strategies affect dehydrogenation time in magnesium-based storage systems. Common approaches include improving the heat transfer structure [64,67], increasing convective heat transfer coefficients [3,44,64,65], boosting effective thermal conductivity [31,65], or enhancing material permeability [66], as detailed in Table 2. The DDDH strategy achieves up to a 57.99 % reduction in dehydrogenation time, which is surpassing most traditional methods. It achieves this by modifying the heating profile during the reaction without altering external system conditions. Moreover, under adiabatic conditions, this time saving comes with no increase in energy use. While increasing convective heat transfer coefficients can improve reaction rates by up to 60.17 %, it also raises energy consumption and cost. This further highlights the advantage of the DDDH approach in delivering efficient and cost-effective dehydrogenation, supporting scalable and sustainable hydrogen storage solutions.

3.7. Evaluating dehydrogenation performance under non-adiabatic scenarios

While the preceding sections focused on adiabatic conditions,

practical implementations must account for ambient heat dissipation. Consequently, thermal management of the hydrogen storage system becomes critical. In this study, five different thermal environments for Model B were evaluated: (I) adiabatic condition; (II-III) conductive heat loss cases with insulation thickness of 0.1 m (thermal conductivities of 0.024 and 0.0322 W/m/K) [68,69] and (IV-V) convective heat transfer cases with external heat transfer coefficients of 1 and 2 W/m²/K, representing typical natural convection environments or weak insulation scenarios. The variation curves of reaction fraction and dehydrogenation temperature under these conditions are shown in Fig. S12 and Table S8. Although the thermal environments introduce some variation in temperature profiles and reaction behavior, the DDDH strategy consistently outperforms the conventional isothermal approach across all cases. Fig. 9 delineates the dehydrogenation energy consumption and time characteristics under isothermal and DDDH strategies, contrasting adiabatic operation, multiple insulation measures and natural convection scenarios.

Fig. 9(a) displays the dehydrogenation energy consumption variations of both strategies under different thermal environments. Under adiabatic conditions, where energy consumption is solely determined by equilibrium temperature, both strategies demonstrate identical energy consumption. When heat dissipation occurs, the continuous heat exchange between the hydrogen storage tank and ambient environment introduces time-dependent energy consumption characteristics. As shown in Fig. 9(b), the reduced duration in high-temperature regions under DDDH implementation significantly impacts the overall dehydrogenation time. Despite environmental heat loss, the DDDH strategy consistently achieves faster hydrogen release, with dehydrogenation time reductions ranging from 57.99 % to 42.44 % across varying thermal conditions. This shorter operational time not only minimizes heat dissipation loss but also enhances the overall thermal utilization, which is critical for large-scale and long-duration hydrogen storage

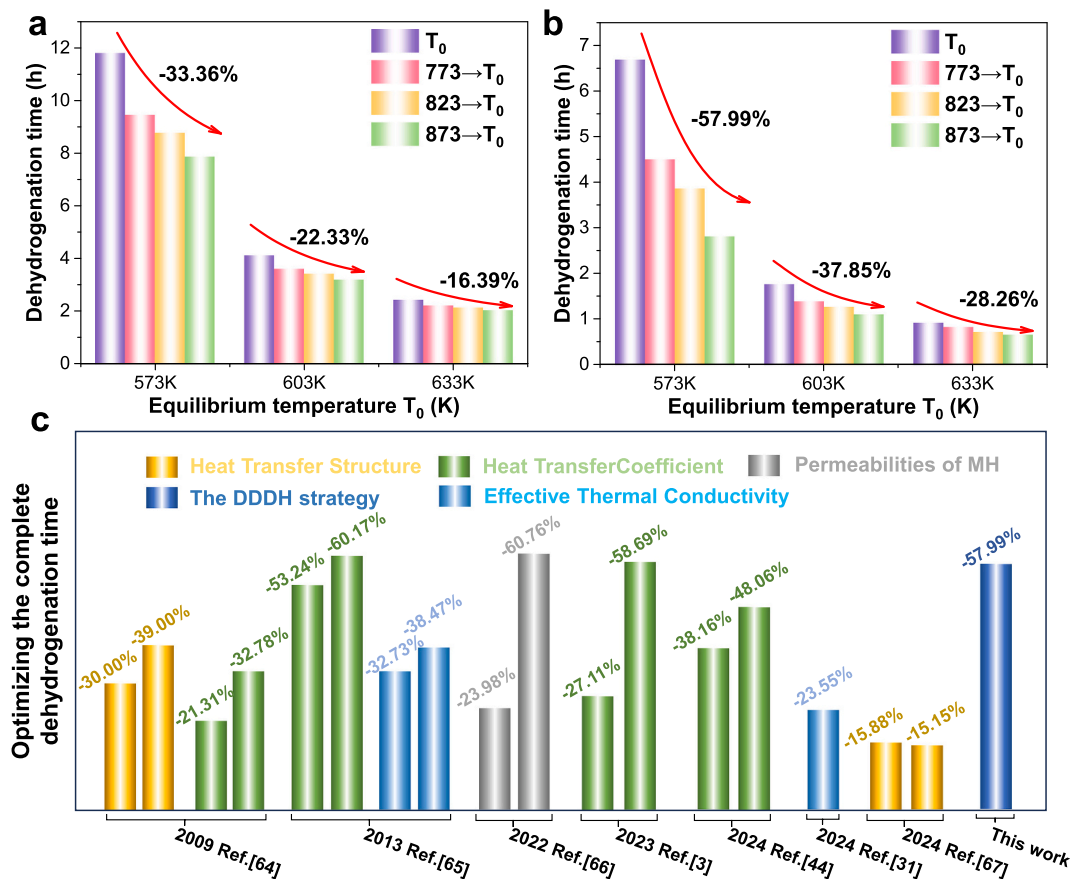


Fig. 8. Time optimization of different dehydrogenation strategies for (a) Model A (without fins) and (b) Model B (with fins). (c) Complete dehydrogenation time optimization compared to other works [3,31,44,64–67].

Table 2
Dehydrogenation rate optimization compared to other works.

Optimization measures	Detailed contents		Dehydrogenation time	Optimized quantity	Ref.
Heat transfer structure	Enhancing heat transfer structures to improve dehydrogenation rates.	Tank	10,000 s	Base Line	[64]
		Exchange pipe	7000 s	39.00 %	
		Pipe and fins	6100 s	30.00 %	
Heat transfer coefficient	Adjusting fluid flow rates in concentric-tube finned tanks to accelerate heat exchange.	40 m/s	6100 s	Base Line	[65]
		80 m/s	4800 s	21.31 %	
		120 m/s	4100 s	32.78 %	
		10 W/m ² /K	5.55 h	Base Line	
Heat transfer coefficient	Modifying the convective heat transfer coefficient to assess its impact on dynamic tank performance.	100 W/m ² /K	2.59 h	53.24 %	[65]
		1000 W/m ² /K	2.21 h	60.17 %	
		0.2 W/m/K	2.55 h	Base Line	
Effective thermal conductivity	Altering effective thermal conductivity to evaluate its influence on reaction behavior.	0.4 W/m/K	1.72 h	32.73 %	[65]
		0.674 W/m/K	1.57 h	38.47 %	
		5.9e-16 m ²	11.01 h	Base Line	
Permeability of MH	Varying material permeability to observe changes in dehydrogenation time.	1e-15 m ²	8.37 h	23.98 %	[66]
		1e-14 m ²	4.35 h	60.76 %	
		0.5 m/s	5.49 h	Base Line	
Heat transfer coefficient	Controlling heat-conducting oil flow rates in large-scale magnesium-based tanks.	1 m/s	4.00 h	27.11 %	[3]
		9 m/s	2.27 h	58.69 %	
		25 m/s	5.75 h	Base Line	
Heat transfer coefficient	Changing Ar gas flow rate in MgH ₂ tanks under zero-gravity design conditions.	50 m/s	3.88 h	32.16 %	[44]
		100 m/s	2.97 h	48.06 %	
		4412 s	4412 s	Base Line	
Effective thermal conductivity	Compacting MgH ₂ into disks to investigate the impact of structural form on reaction time.	Disks	3373 s	23.55 %	[31]
		0 mm	3512 s	Base Line	
Heat transfer coefficient	Adjusting the flow layer thickness to optimize heat and mass transfer performance.	5 mm	2954 s	15.88 %	[67]
		10 mm	2980 s	15.15 %	
		573 K	6.69 h	Base Line	
The DDDH strategy	Implementing a demand-driven heating strategy based on the burst effect to match energy input with kinetic demand.	From 873 K to 573 K	2.81 h	57.99 %	This work

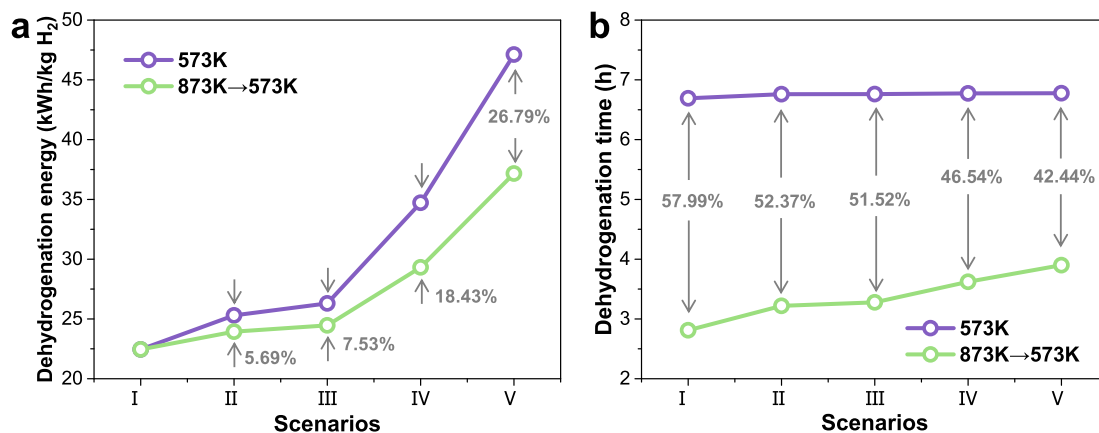


Fig. 9. Changes in (a) dehydrogenation energy consumption and (b) dehydrogenation time for isothermal dehydrogenation strategy versus DDDH strategy under different thermal environments for Model B.

applications. Notably, increasing heat dissipation exacerbates the energy demand disparity between isothermal and the DDDH strategy. These findings further validate the robustness and practical applicability of the DDDH strategy under realistic, non-ideal conditions where thermal losses are inevitable. However, the increased energy and time requirements under high heat transfer scenarios highlight the need for effective thermal insulation and environmental shielding, especially when deploying MgH₂-based storage systems in stationary or grid-integrated energy infrastructures.

4. Conclusion

In this study, a novel demand-driven dynamic heating (DDDH) strategy that synchronizes thermal supply with reaction-stage-specific energy demands in MgH₂ dehydrogenation was proposed. The DDDH strategy originates from dynamic dehydrogenation kinetics of MgH₂ based on its burst effect, constructing a bridge between materials science and thermal management engineering. The DDDH strategy was applied to two typical hydrogen storage tanks (with and without fins) through multi-physics field simulation. By targeting both kinetic limitations and system-level thermal inefficiencies, this work provides a new technical pathway for enhancing solid-state hydrogen storage systems geared toward large-scale energy applications. The DDDH strategy can simultaneously reduce dehydrogenation time, reduce energy consumption, and enhance exergy efficiency. The key findings are summarized as follows:

- (1) Through segmented fitting of the experimental dehydrogenation kinetics curve, the variation curves of reaction rate parameters (activation energy and pre-exponential factor) with the dehydrogenation progress were obtained. Specifically, the dehydrogenation energy barrier is initially high at the onset of the reaction, gradually decreasing and ultimately stabilizing as the reaction progresses toward equilibrium, which is highly consistent with the burst effect in theoretical.
- (2) The DDDH strategy can reduce the energy consumption of dehydrogenation reactions while enhancing exergy efficiency. At peak and equilibrium temperatures of 873 K and 573 K, energy savings for the two models reached 0.31 and 0.67 kWh/kg H₂, representing 1.46 % and 2.98 % reductions, respectively. Notably, energy savings exhibited a positive correlation with equilibrium temperature: when equilibrium temperature increased to 603 K, the savings further rose to 2.87 % and 3.49 % for the respective models. Concurrently, exergy efficiency improved by 1.26 % and 3.23 % compared to the isothermal heating strategy.

- (3) The DDDH strategy can significantly reduce the dehydrogenation time. Dehydrogenation duration decreased proportionally with increasing peak temperature but inversely correlated with equilibrium temperature elevation. At peak and equilibrium temperatures of 873 K and 573 K, respectively, the two models achieved time reductions of 33.36 % and 57.99 %. These results strongly support the potential of the DDDH strategy for rapid hydrogen release in practical, high-capacity storage systems.
- (4) The DDDH strategy further demonstrates superior performance in both dehydrogenation duration and energy consumption under non-adiabatic conditions. However, excessive external heat transfer incurs significant energy penalties, consequently necessitating effective thermal insulation implementation in practical engineering applications.

This study contributes a scalable thermal management strategy that combines energy supply-demand matching with the intrinsic kinetics of MgH₂, aiming to serve the practical demands of stationary and grid-level hydrogen energy storage. This strategy enables simultaneous enhancement of dehydrogenation rate and system-level energy/exergy efficiencies without requiring additional equipment. Future work will involve experimental validation of the DDDH strategy, with systematic measurements focusing on system durability and material cyclability under dynamic operating conditions. The success of the DDDH strategy highlights its applicability as a robust framework for next-generation solid-state hydrogen storage systems, particularly those intended for large-scale and long-duration energy storage infrastructure.

CRediT authorship contribution statement

Jianghao Cai: Writing – review & editing, Writing – original draft, Software, Data curation. **Yutong Jiang:** Software, Investigation. **Tonggao Yao:** Data curation, Writing – review & editing. **Xiaotian Tang:** Investigation, Software. **Yuxuan Liu:** Software, Visualization. **Zhuoran Xu:** Formal analysis. **Xiaojun Zhao:** Resources, Software. **Bingdong Zhang:** Methodology, Conceptualization. **Zhengyang Gao:** Supervision, Project administration. **Weijie Yang:** Writing – review & editing, Supervision, Funding acquisition.

Declaration of Generative AI and AI-assisted technologies in the writing process

During the preparation of this work, the authors used ChatGPT in order to improve language expression and check grammar. After using this tool, the authors reviewed and edited the content as needed and take full responsibility for the content of the publication.

Declaration of competing interest

The authors declare that they have no known competing financial interests or personal relationships that could have appeared to influence the work reported in this paper.

Acknowledgements

This work was funded by the Natural Science Foundation of Hebei Province (E2023502006) and Fundamental Research Fund for the Central Universities (2025MS131).

Appendix A. Supplementary data

Supplementary data to this article can be found online at <https://doi.org/10.1016/j.est.2025.117495>.

Data availability

Data will be made available on request.

References

- M.D. Allendorf, V. Stavila, J.L. Snider, et al., Challenges to developing materials for the transport and storage of hydrogen, *Nat. Chem.* 14 (11) (2022) 1214–1223.
- X. Zhang, S. Ju, C. Li, et al., Atomic reconstruction for realizing stable solar-driven reversible hydrogen storage of magnesium hydride, *Nat. Commun.* 15 (1) (2024) 2815.
- X. Lin, C.L. Yin, L. Ren, et al., A one- and three-dimensional coupled model and simulation investigation for the large-scale oil-heating type Mg-based hydrogen storage tank, *Chem. Eng. J.* 472 (2023) 144943.
- S. Dong, H. Liu, X. Liu, et al., Facile dehydrogenation of MgH₂ enabled by γ -graphyne based single-atom catalyst, *J. Energy Storage* 74 (2023) 109484.
- L. Schlapbach, A. Züttel, Hydrogen-storage materials for mobile applications, *Nature* 414 (6861) (2001) 353–358.
- D. Li, F. Huang, B. Ren, et al., Microstructure and hydrogen storage properties of the Mg_{2-x}Y_xNi_{0.9}Co_{0.1} (x=0, 0.2, 0.3, and 0.4) alloys, *Sci. Rep.* 14(1):905 (2024).
- J. Wo, W. Yang, Fullerene nano-confinement enables ultra-low dehydrogenation temperature of MgH₂: A DFT-based theoretical prediction, *Int. J. Hydrogen Energy* 146 (2025) 149987.
- L. Ren, Y. Li, N. Zhang, et al., Nanostructuring of Mg-based hydrogen storage materials: recent advances for promoting key applications, *Nano-Micro Lett.* 15 (2023) 93.
- J. Karst, F. Sterl, H. Linnenbank, et al., Watching in situ the hydrogen diffusion dynamics in magnesium on the nanoscale, *Sci. Adv.* 6(19):eaaz0566 (2020).
- N. Klopčić, I. Grimmer, F. Winkler, et al., A review on metal hydride materials for hydrogen storage, *J. Energy Storage* 72 (Part B) (2023) 108456.
- H. Jiang, Z. Ding, Y. Li, et al., Hierarchical interface engineering for advanced magnesium-based hydrogen storage: synergistic effects of structural design and compositional modification, *Chem. Sci.* 16 (2025) 7610.
- Q. Li, X. Lin, Q. Luo, et al., Kinetics of the hydrogen absorption and desorption processes of hydrogen storage alloys: a review, *Int. J. Miner. Metall. Mater.* 29 (2022) 32–48.
- Z. Ding, Y. Li, H. Yang, et al., Tailoring MgH₂ for hydrogen storage through nanoengineering and catalysis, *J. Magnes. Alloy* 10 (2022) 2946–2967.
- H. Yang, Z. Ding, Y. Li, et al., Recent advances in kinetic and thermodynamic regulation of magnesium hydride for hydrogen storage, *Rare Metals* 42 (9) (2023) 2906–2927.
- Z. Bao, F. Yang, Z. Wu, et al., Simulation studies on heat and mass transfer in high-temperature magnesium hydride reactors, *Appl. Energy* 112 (2013) 1181–1189.
- Z. Bao, Performance investigation and optimization of metal hydride reactors for high temperature thermochemical heat storage, *Int. J. Hydrog. Energy* 40 (16) (2015) 5664–5676.
- Z. Wu, F. Yang, L. Zhu, et al., Improvement in hydrogen desorption performances of magnesium based metal hydride reactor by incorporating helical coil heat exchanger, *Int. J. Hydrog. Energy* 41 (36) (2016) 16108–16121.
- A. Mathew, N. Nadim, T.T. Chandratilleke, et al., Performance analysis of a high-temperature magnesium hydride reactor tank with a helical coil heat exchanger for thermal storage, *Int. J. Hydrog. Energy* 46 (1) (2021) 1038–1055.
- H. Chang, Y.B. Tao, H. Ye, Numerical study on hydrogen and thermal storage performance of a sandwich reaction bed filled with metal hydride and thermochemical material, *Int. J. Hydrog. Energy* 48 (52) (2023) 20006–20019.
- L. Shao, X. Lin, L. Bian, et al., Engineering control strategy of hydrogen gas direct-heating type Mg-based solid state hydrogen storage tanks: a simulation investigation, *Appl. Energy* 375 (2024) 124134.
- C. Yan, X. Lu, J. Zheng, et al., Dual-cation K₂TaF₇ catalyst improves high-capacity hydrogen storage behavior of MgH₂, *Int. J. Hydrog. Energy* 48 (15) (2023) 6023–6033.
- L. Wang, L. Zhang, X. Lu, et al., Surprising cocktail effect in high entropy alloys on catalyzing magnesium hydride for solid-state hydrogen storage, *Chem. Eng. J.* 465 (2023) 142766.
- S. Guemou, F. Wu, P. Chen, et al., Graphene-anchored Ni₆MnO₈ nanoparticles with steady catalytic action to accelerate the hydrogen storage kinetics of MgH₂, *Int. J. Hydrog. Energy* 48 (62) (2023) 23943–23955.
- M. Song, F. Wu, Y. Jiang, et al., Optimizing FeCoNiCrTi high-entropy alloy with hydrogen pumping effect to boost de/hydrogenation performance of magnesium hydride, *Rare Metals* 43 (2024) 3273–3285.
- C. Lu, H. Liu, L. Xu, et al., Two-dimensional vanadium carbide for simultaneously tailoring the hydrogen sorption thermodynamics and kinetics of magnesium hydride, *J. Magnes. Alloy* 10 (4) (2022) 1051–1065.
- T. Yang, Q. Li, N. Liu, et al., Improved hydrogen absorption and desorption kinetics of magnesium-based alloy via addition of yttrium, *J. Power Sources* 378 (2018) 636–645.
- J. Kapischke, J. Hapke, Measurement of the effective thermal conductivity of a Mg–MgH₂ packed bed with oscillating heating, *Exp. Thermal Fluid Sci.* 17 (4) (1998) 347–355.
- C. Zhou, C. Hu, Y. Li, et al., Crystallite growth characteristics of Mg during hydrogen desorption of MgH₂, *Prog. Nat. Sci. Mater. Int.* 30 (2) (2020) 246–250.
- S. Dong, C. Li, J. Wang, et al., The “burst effect” of hydrogen desorption in MgH₂ dehydrogenation, *J. Mater. Chem. A* 10 (42) (2022) 22363–22372.
- C. Li, W. Yang, H. Liu, et al., Picturing the gap between the performance and US-DOE’s hydrogen storage target: a data-driven model for MgH₂ dehydrogenation, *Angew. Chem. Int. Ed.* 63 (28) (2024) e202320151.
- Y. Ye, Z. Zhang, J. Liu, et al., Experiment and simulation study on transfer phenomena and performance optimization of MgH₂ based hydrogen storage reactors, *Int. J. Hydrog. Energy* 86 (2024) 649–661.
- F. Yang, X. Cao, Z. Zhang, et al., Assessment on the long term performance of a LaNi₅ based hydrogen storage system, *Energy Procedia* 29 (2012) 720–730.
- D. Lanbaran, C. Wang, C. Wen, et al., Modeling the impact of temperature-dependent thermal conductivity on hydrogen desorption from magnesium hydride, *Int. J. Hydrog. Energy* 138 (2025) 491–508.
- A. Khawam, D.R. Flanagan, Solid-state kinetic models: basics and mathematical fundamentals, *J. Phys. Chem. B* 110 (35) (2006) 17315–17328.
- Z. Tian, Z. Wang, P. Yao, et al., Hydrogen storage behaviors of magnesium hydride catalyzed by transition metal carbides, *Int. J. Hydrog. Energy* 46 (80) (2021) 40203–40216.
- T. Forde, J. Maehlen, V. Yartys, et al., Influence of intrinsic hydrogenation/dehydrogenation kinetics on the dynamic behavior of metal hydrides: a semi-empirical model and its verification, *Int. J. Hydrog. Energy* 32 (8) (2007) 1041–1049.
- C. Chung, C. Ho, Thermal–fluid behavior of the hydriding and dehydriding processes in a metal hydride hydrogen storage canister, *Int. J. Hydrog. Energy* 34 (10) (2009) 4351–4364.
- T. Shi, H. Xu, C. Qi, et al., Multi-physics modeling of thermochemical heat storage with enhance heat transfer, *Appl. Therm. Eng.* 198 (2021) 117508.
- X. Han, H. Xu, C. Zhao, Design and performance evaluation of multi-layered reactor for calcium-based thermochemical heat storage with multi-physics coupling, *Renew. Energy* 195 (2022) 1324–1340.
- A. Chaise, P. De Rango, P. Marty, et al., Experimental and numerical study of a magnesium hydride tank, *Int. J. Hydrog. Energy* 35 (12) (2010) 6311–6322.
- C.S. Wang, J. Brinkerhoff, Advances in mathematical modeling of hydrogen adsorption and desorption in metal hydride beds with lattice Boltzmann method, *Int. J. Hydrog. Energy* 45 (56) (2020) 32179–32195.
- S. Mellouli, F. Askri, T. Alqahtani, et al., Feasibility study of a metal hydride-based solar thermal collector system, *Case Stud. Therm. Eng.* 61 (2024) 105005.
- S. Mellouli, F. Askri, T. Alqahtani, et al., Numerical assessment of a thermal energy storage system based on a metal hydride reactor and a mechanical hydrogen compressor, *Appl. Therm. Eng.* 243 (2024) 122670.
- X. Lin, Z. Zhang, L. Bian, et al., Using magnesium hydride as the future dual-mode propellant for spacecraft: a simulation investigation, *Chem. Eng. J.* 500 (2024) 157410.
- C. Zhao, J. Yan, X. Tian, et al., Progress in thermal energy storage technologies for achieving carbon neutrality, *Carbon Neutrality* 2 (2023) 10.
- J. Yan, Y. Mo, C. Zhao, et al., Preparation and parameter optimization of thermochemical heat storage materials with high cyclic stability, *Sol. Energy Mater. Sol. Cells* 268 (2024) 112749.
- A. Bejan, Two thermodynamic optima in the design of sensible heat units for energy storage, *J. Heat Transf. Trans. Asme* 100 (1978) 708–712.
- L. Kalapala, J. Devanuri, Energy and exergy analyses of latent heat storage unit positioned at different orientations—an experimental study, *Energy* 194 (2020) 116924.
- L. Kalapala, J. Devanuri, Effect of orientation on thermal performance of a latent heat storage system equipped with annular fins – an experimental and numerical investigation, *Appl. Therm. Eng.* 183 (2) (2021) 116244.
- S. Seddegh, X. Wang, M. Joybari, et al., Investigation of the effect of geometric and operating parameters on thermal behavior of vertical shell-and-tube latent heat energy storage systems, *Energy* 137 (2017) 69–82.
- J. Yin, Y. Yan, M. Miao, et al., Diamond with Sp²-Sp³ composite phase for thermometry at Millikelvin temperatures, *Nat. Commun.* 15 (2024) 3871.
- B. Chaker, B. Sihem, H.D. Mohamed, et al., Dynamic study of a new design of a tanks based on metallic hydrides, *Int. J. Hydrog. Energy* 43 (3) (2018) 1566–1576.
- Z. Dong, Y. Wang, H. Wu, et al., A design methodology of large-scale metal hydride reactor based on schematization for hydrogen storage, *J. Energy Storage* 49 (2022) 104047.

- [54] W. Yang, H. Ge, T. Yao, et al., Promotion mechanisms of LiBH_4 dehydrogenation dominated by charge redistribution, *J. Mater. Chem. A* 13 (2025) 1014–1022.
- [55] H. Wan, X. Yang, S. Zhou, et al., Enhancing hydrogen storage properties of MgH_2 using FeCoNiCrMn high entropy alloy catalysts, *J. Mater. Sci. Technol.* 149 (2023) 88–98.
- [56] X. Lin, D. Sun, S. Chen, et al., Numerical analysis on pulverization and self-densification for hydrogen storage performance of a metal hydride tank, *Appl. Therm. Eng.* 161 (2019) 114129.
- [57] X. Lin, Q. Zhu, H. Leng, et al., Numerical analysis of the effects of particle radius and porosity on hydrogen absorption performances in metal hydride tank, *Appl. Energy* 250 (2019) 1065–1072.
- [58] S. Mellouli, F. Askri, H. Dhaou, et al., A study of the thermal behavior of a deformable metal-hydride bed, *Int. J. Hydrog. Energy* 41 (3) (2016) 1711–1724.
- [59] L. Liu, K. Wang, H. Luo, et al., Fin structure optimization for improving heat transfer efficiency and hydrogen absorption rate of metal hydride hydrogen storage tank, *Int. J. Hydrog. Energy* 65 (2024) 362–374.
- [60] V. Keshari, M.P. Maiya, Design and investigation of hydriding alloy based hydrogen storage reactor integrated with a pin fin tube heat exchanger, *Int. J. Hydrog. Energy* 43 (14) (2018) 7081–7095.
- [61] S. Xing, S. Zhai, L. Chen, et al., Insights into carbon-based materials for catalytic dehydrogenation of low-carbon alkanes and ethylbenzene, *Front. Chem. Sci. Eng.* 17 (2023) 1623–1648.
- [62] Rami S. El-Emam, I. Dincer, et al., Energy and exergy analyses of an integrated SOFC and coal gasification system, *Int. J. Hydrog. Energy* 37 (2) (2012) 1689–1697.
- [63] T. Li, X. Xiang, S. Liu, et al., Analysis of dual fluidized bed gasification process based on the difference between energy efficiency and exergy efficiency, *Energy Convers. Manag.* 326 (2025) 119475.
- [64] C. Chung, C. Lin, Prediction of hydrogen desorption performance of Mg_2Ni hydride reactors, *Int. J. Hydrog. Energy* 34 (23) (2009) 9409–9423.
- [65] H. Mâad, F. Askri, S. Ben, et al., Numerical investigation of heat and mass transfer during the desorption process of an $\text{Mg}_2\text{Ni-H}_2$ reactor, *Int. J. Hydrog. Energy* 38 (11) (2013) 4597–4610.
- [66] T. Shi, H. Xu, H. Ke, et al., Thermal transport of charging/discharging for hydrogen storage in a metal hydride reactor coupled with thermochemical heat storage materials, *Energy Convers. Manag.* 273 (2022) 116421.
- [67] W. Wang, M. Wang, J. Wang, et al., Numerical study on hydrogen desorption performance of a new MgH_2 solid-state hydrogen storage device, *Int. J. Hydrog. Energy* 86 (2024) 530–541.
- [68] L. An, J. Armstrong, Y. Hu, et al., High temperature ceramic thermal insulation material, *Nano Res.* 15 (2022) 6662–6669.
- [69] X. Zhang, F. Wang, L. Dou, et al., Ultrastrong, superelastic, and lamellar multiarch structured $\text{ZrO}_2\text{-Al}_2\text{O}_3$ nanofibrous aerogels with high-temperature resistance over 1300 °C, *ACS Nano* 14 (11) (2020) 15616–15625.